SAND2017-0560C

Characterizing Low-Z Erosion and Deposition in the DIII-D Divertor Using Aluminum

C.P. Chrobak[a], G.R. Tynan[b], R.P. Doerner[b], P.C. Stangeby[c], W.R. Wampler[d], D.L. Rudakov[b], G.M. Wright[g], T. Abrams[e], R. Ding[e], J.D. Elder[c], J. Guterl[e], H.Y. Guo[a], C. Lasnier[f], D.M. Thomas[a], A.W. Leonard[a], D.A. Buchenauer[d], A.G. McLean[f], J.G. Watkins[d]

[a] *General Atomics, PO Box 85608, San Diego, CA 92186-5608, USA*

[b] *University of California San Diego, 9500 Gilman Drive, La Jolla, CA 92093-0417, USA*

[c] *University of Toronto, Institute for Aerospace Studies, Toronto, M3H 5T6, Canada*

[d] *Sandia National Laboratory, P.O. Box 5800, Albuquerque, NM 87185, USA*

[e] *Oak Ridge Associated Universities, Oak Ridge, Tennessee, 37830, USA*

[f] *Lawrence Livermore National Laboratory, 7000 East Avenue, Livermore, CA 94550, USA*

[g] *Massachusetts Institute of Technology, 77 Massachusetts Ave, Cambridge, Massachusetts 02139, USA*

Abstract

We present measurements and modeling of aluminum erosion and redeposition experiments in separate helium and deuterium low power, low density L-mode plasmas at the outer divertor strike point of DIII-D to provide a low-Z material benchmark dataset for tokamak erosion-deposition modeling codes. Coatings of Al ~100nm thick were applied to ideal (smooth) and realistic (rough) surfaces and exposed to repeat plasma discharges using the DiMES probe. Redeposition and re-erosion in all cases was primarily in the downstream toroidal field direction, evident from both in-situ spectroscopic and post-mortem non-spectroscopic measurements. The gross Al erosion yield in He plasmas was 4.7x higher than in similar D plasmas, consistent with the expected physical sputtering yields. Al I emission during the exposure suggests the erosion yield for redeposited material is significantly higher than the as-deposited material. The fraction of total eroded material found redeposited on the rough substrate was proportional to the total eroded material and was much higher than on the smooth substrate, which is attributed to Al redeposition in areas shadowed from re-erosion such as pores. A simple model

for erosion and redeposition is presented that reproduces many of the observed results in these experiments, including toroidal erosion asymmetry, the high rate of re-erosion, and the increased fraction of metal found redeposited near the original coating on rough vs. smooth substrates. The model uses theoretically calculated sputtering yields, calculates surface composition changes and erosion rates in time, and assumes a spatial distribution of redeposition with a trapping parameter to account for redeposition in hidden areas. Fitting the model to the measurement finds the total redeposition fraction increases with higher plasma temperature (~30% for 15-20eV plasmas, and ~45% for 25-30eV plasmas), and on rough substrates, 50% of the redeposited material is trapped in pores.

PSI-22 Keywords: Erosion, Deposition, Low-Z, Roughness, Divertor, Aluminum

**Corresponding author address:* General Atomics, MS 34-218, 3483 Dunhill St, San Diego, CA 92121

**Corresponding author e-mail:* chrobak@fusion.gat.com

Presenting author: Christopher Chrobak

Presenting author e-mail: chrobak@fusion.gat.com

1. Introduction

Predictions of the net erosion and lifetime of the ITER Be first wall have high uncertainty primarily due to large variations in the measured and predicted sputtering yields of Be [1]. It is expected that as eroded first wall material will migrate to the divertor, its re-erosion and re-deposition will lead to material mixing and degraded thermal and mechanical properties of the tungsten divertor [2] [3], and its accumulation in regions of net deposition will lead to tritium retention by co-deposition. Divertor plasma contact with low-Z materials in ITER is expected in the secondary (upper) divertor where most of the actual erosion [atoms/s] will occur, and in the primary divertor where re-erosion of deposited Be and other low-Z impurities is expected. Previous experiments have been conducted on EAST and JET to benchmark modeling codes for low-Z net erosion/deposition in limiter-type plasma contact (C in EAST [4,5], Be in JET

[6]). This study presents a controlled measurement of low Z material erosion-deposition in divertor-type plasma contact using Al in DIII-D.

Redeposition of eroded material is primarily driven by the ionization process and, in the tokamak divertor, the magnetic and electric field within the magnetic pre-sheath (MPS) region [7]. For Al, the ionization length is on the same order (~0.5-2mm) as its ion gyro radius and the scale lengths of the DIII-D divertor magnetic pre-sheath. For this reason, the dominant redeposition process is expected to be driven by the ion-plasma interaction and depend on the structure of the sheath and MPS. Al also has easily measurable neutral and ionized spectroscopic emission, a uniqueness from background materials in DIII-D, and shares similar hydride and oxide chemistry with Be [8]. These properties together make Al a relevant candidate material for studying the underlying physics of the plasma-controlled redeposition process important to Low-Z material erosion and deposition.

In this study, we used well-diagnosed simple as possible attached L-mode DIII-D divertor plasmas for consistency with previous net and gross erosion measurements of other materials (W, Mo), and used both He and D species to modify the gross erosion rates and background carbon impurity fraction. Thin film Al coated samples were exposed using the DiMES manipulator [9]. Two complementary techniques for measuring erosion were used in these experiments: post-mortem Rutherford Backscattering spectroscopy (RBS) measurements of film thickness; and spectroscopic imaging to monitor erosion rates during plasma exposure. Al erosion by background C impurity ions was estimated by comparing the erosion of W in similar low density L-mode plasmas. A simple erosion-redeposition model, presented in section 3.2, reproduces many of the observations and was used to interpret the resulting erosion and redeposition profiles and determine the redeposition fraction.

2. Material and Methods

2.1. Exposure Conditions

All samples were exposed near the outer strike point (OSP) of a series of DIII-D lower single null low density attached deuterium and helium L-mode plasmas using the DiMES manipulator [10]. The plasma parameters were chosen to maintain simple-as-possible attached divertor conditions over the sample, similar to those used and modeled in previous erosion-deposition studies [11]. Each sample accumulated between 6 and 25 seconds of steady-state plasma exposure, achieved by using repeat steady plasmas and OSP position control. The OSP was maintained 7-20mm inboard of the sample during the steady state phase of the discharge, and 50mm outboard of the sample during the transient phases. Infrared camera and Langmuir probe heat flux measurements indicate average sample surface temperature reached ~300-400C in each exposure for case Al1, but remained below 100C for cases Al4 and Al5 due to the lower ion temperature and fluxes in those cases. A compilation of the average plasma conditions during each sample exposure is listed in **Table 1**. The coating geometry for each sample, described in **Figure 1**, included both large and small areas to vary the redeposition fraction and determine the gross erosion rate non-spectroscopically by post-mortem RBS analysis as in [12,13].

Charge exchange recombination (CER) spectroscopy shows that carbon is the dominant plasma impurity, with steady concentrations ranging from 0.5-1.5% throughout the core and pedestal. The small background carbon impurity fraction in DIII-D has a significant impact on the observed erosion rates and mixed material formation. We have estimated the Al erosion by carbon ions and the carbon impurity flux to the sample based on post mortem measurements of gross W erosion in similar plasma conditions. Erosion of W in these plasma conditions is almost entirely due to C ion sputtering. For the Al1 case, a separate but similar plasma exposure of W [10] was used; and for the Al5 case, the simultaneous exposure of a W spot on the sample was used. C ion sputtering yields were calculated assuming a single C^{3+} ion state impacting the sample at 45-degree incidence angle at an impact energy determined from the sum

of the average ion thermal energy and sheath potential drop, $E_{Impact} \approx 3Z_iT_e + 2T_e$ [14]. Modeling of similar plasmas [15] has shown that erosion results are not significantly different when using a distribution of ion states and energies. The gross erosion of Al by C ion sputtering was estimated by scaling the gross W erosion yield at similar plasma conditions by the ratio of their sputtering yields $Y_{C\rightarrow Al}/Y_{C\rightarrow W}$. The resulting C ion impurity fraction was calculated based on the fraction of C^{3+} ions required to achieve that erosion rate. It is counter-intuitive that the C fraction estimate in the Al5, He plasma case is ~3x higher than in the Al1, D plasma case, since the physical sputtering yield of ~75 eV He > C (0.06) is slightly less than the expected chemical + physical sputtering yield of ~150eV D > C (0.07). However, the CII (392nm) line intensity seen by the multichord divertor spectrometer (MDS) was also ~3x higher in the He plasma case.

Table1: Averaged local plasma parameters for each sample case measured as shown below. Sample Al4 parameters varied by ~30% during exposure time due to strike point position shifts, as described in more detail in [16]**.**

Case	Plasma	Time s	Local B_T T	B_{incl} deg	T_e eV	n_e x10^{13} cm^{-3}	Heat Flux W/cm^2	Ped C% [CER]	CII 392nm intens	C3+% est.	DIII-D Shots
Al1	D	14	2.3	-1.65	29.6[a] 25.1[b]	1.16[a] 1.34[b]	64.0[LP] 162[IR]	0.63%	7	0.96%	148673-148677
Al4	D	12.6	2.2	-1.25	16.0[a] 18.4[b]	0.96[a] 2.79[b]	16[LP] 5.5[IR]	0.78%	3.2-5.7	0.8-1.6%[c]	153860-153864
Al5	He	6.2	2.18	-1.4	14.8[a] 14.8[b]	1.1[a] 1.7[b]	18.2[LP] 5.7[IR]	n/a	17.5	2.8%	158446-158448

a. Langmuir Probes; b. Thomson scattering chord 10mm above floor; c. Scaled from Al1 and Al5 cases using CII intensity, IR. Divertor viewing infrared camera viewing at 60 degrees toroidal, LP. Langmuir probe calculated heat flux using sheath transmission factor of 7

2.2. Surface Characterization

Vacuum evaporative deposition was used to coat Al films to an initial thickness of 80-130nm onto different substrates. Case Al1 used a 500nm CVD carbon-coated Si substrate with a negligible (<2nm) surface roughness. Cases Al4 and Al5 used an ATJ graphite substrate. The graphite, although polished, had pores 5-50um in size covering ~10% of the surface (Figure 2b shows the analyzed size distribution). Surface roughness and porosity was characterized using profilometry, backscattering electron (BEI) and secondary electron (SEI) image analysis (Figure 2). Excluding the pores, the graphite surface had an average roughness of 600nm. Film thickness and composition was measured using He and proton RBS.

Average oxygen content in the film was ~10%, with a ~20nm oxygen-rich surface layer. Both SEM and optical profilometry show the coating to be conformal to the substrate morphology.

3. Results

3.1. Measurements of Net and Gross Erosion in He and D Plasmas

The erosion and redeposition rates in each case were measured by post-mortem RBS analysis of multiple points along radial and toroidal profiles across the samples. Higher erosion rates observed from small areas on the upstream side of the sample and near the coating edges, along with the toroidal asymmetry of the redeposited material indicate that the eroded material is redeposited on the order of a few mm from the source, and primarily in the downstream toroidal field direction. Toroidal profiles of the net erosion and deposition were interpreted by fitting a simple erosion-redeposition model (described in section 3.2) to the data (Data and Fits shown in figure 6). The model fit determined that the overall fraction of eroded material returning to the surface is found to increase with higher plasma temperature (~30% for 15-20eV He and D plasmas, and ~45% for 25-30eV plasmas), consistent with the stronger ionization rate and electric field expected. Radial profiles show a slight inward bias, consistent with the ExB drifts direction, although radial variation of the plasma parameters (ne, Te, Flux, C%) complicates the interpretation. More comprehensive modeling of the plasma driven redeposition process would be needed to draw firmer conclusions and is beyond the scope of this report.

Samples Al4 and Al5 each had the same fraction (5-6%) of net eroded material found redeposited 5mm outside the original coating area. This is despite Al5 having a ~5x higher gross erosion rate (due to higher He sputtering yield) and lower temperature plasma which should result in longer ionization lengths and less local redeposition. For sample Al1, a much lower fraction of net eroded material was found (~0.5%), despite it being exposed to higher temperature plasma. This apparent discrepancy may be explained by the rougher, porous substrate common between samples Al4 and Al5. Eroded material deposited deep into pores becomes trapped, or hidden from incident ions.

This type of localized net deposition has been observed and modeled for tungsten in various tokamaks [17–19], and may be caused if the redeposited Al has a steeper average incidence angle than the eroding ions or if by sputtering from flux-facing pore edges with line-of-sight deposition into the pores. The latter may explain the non-isotropic appearance of the exposed coating, appearing brighter when illuminated from the upstream side and darker when illuminated from the downstream side (Figure 1b). RBS spectra on the exposed sample show a broadening of the low energy tail of the Al peak which is more pronounced in regions that appeared visibly darker and had lower net erosion. The broadening indicates an increase in the distribution of thicknesses within the ~1mm diameter measurement area, due to net erosion between and net deposition inside pores (Figure 3).

Gross erosion was also measured using spectroscopic imaging of neutral Al (AlI, 396 nm) emission during the exposures. Emission from areas outside the initial sample indicates re-erosion of redeposited Al, and is seen to occur primarily in the downstream toroidal field direction (Figure 4). In each case, the AlI emission was found to increase during first few seconds of plasma exposure, while plasma parameters remained nearly constant. Although some of this may be attributed to oxide removal or surface reflectivity increase, the fact that it occurs primarily in regions of higher redeposition suggests this is due to an enhanced erosion rate for redeposited material, as other studies have suggested for C in JET [20], Mo in DIII-D[15], and Be in PISCES-B[21].

Table 2. Summary of erosion rates measured from net (~10mm) and gross(~1mm stripe) areas. Gross erosion measurement for Al1 was not possible due to complete removal of 1mm spot. Model fit results to net, gross, and net:gross erosion ratio are shown, along with fitting parameters used.

Case	Ion Flux (perp) $x10^{18}cm^{-2}s^{-1}$	Gross Erosion nm/s	Net Erosion nm/s	Gross Yield At/ion	Net:Gr Ratio	SAP model fit parameters					λ_{ioniz} mm	R_L mm
						Dep %	Trap %	Yield %	W	Skew		
Al1	1.88[a]	>5.7[a] 7.1[a]	5.1[a] 5.4[b]	>.018[a] .023[b]	>0.88[a] 0.75[b]	45%	0%	71%	1.5	0.65	1.32	0.42
Al4	0.82-.91[a]	2.5a 2.7b	2.0a 2.5b	.017[a] .019[b]	0.81[a] 0.91[b]	30%	50%	57%	1.5	0.5	1.58	0.44
Al5	1.08[a]	14[a] 12.0[b]	12[a] 10.8[b]	.080[a] .067[b]	0.86[a] 0.90[b]	30%	50%	67%	4.5	0.35	1.78	0.47

a. non-spectroscopic RBS measurement
b. SAP model result

3.2. SAP Erosion-Deposition Model

A model of the dynamic erosion and deposition process that includes multi-step re-erosion has been developed to interpret the erosion measurements. It builds on a previous version developed by Wampler after similar DiMES experiments found a lower than expected fraction net eroded Mo material redeposited on DiMES probe and the high concentration of carbon found on the Mo surface in net erosion [22,23]. The model balances the incoming and outgoing fluxes of target materials, carbon and aluminum in this case, assuming sputtering from a mixed material surface layer and a spatially defined redeposition probability distribution function. Surface material mixing resulting from carbon implantation and Al redeposition are approximated by balancing the net erosion and deposition fluxes of Al and carbon into a homogeneous layer of a depth roughly equal to the implantation depth of carbon ions in the material (~1-2nm for 200-400eV C in Al). The resulting effect is that the surface rapidly (within the first few hundred ms) reaches an equilibrium concentration, similar to what is predicted by more advanced simulation codes such as ITMC/DYN [15].

The model also accounts for a fraction of the redeposited material accumulating in surface traps such as pores or cracks. This material is not re-eroded and does not contribute to the concentration of the mixed eroding surface layer. However, it is integrated in the post-mortem measurement of film thickness and would explain the broadening RBS peaks as discussed earlier. Material not redeposited is considered lost to the plasma. With these assumptions, the model is able to reproduce the post-mortem measured erosion/deposition rates astonishingly well (Figure6), using a set of fitting parameters to adjust the erosion, deposition, and trapping rates, as described below.

Sputtering yields calculated for pure element targets using the TRIM.SP modeling code [24] and weighted by the concentration of that element in the mixed surface layer were used. We included sputtering by singly charged D or He ions, a 1-3% C^{3+} impurity (as discussed earlier in section 2.1), and self-sputtering by the redeposited flux of Al^{+}. A single 45-degree incidence angle for all sputtering ions

was used, and the ion impact energy was estimated as discussed earlier using $E_{Impact} \approx 3Z_iT_e + 2T_e$ [14]. Plasma parameters were taken from measurements as described in section 2.1. Secondary effects such as flux-dependent surface saturation with the main sputtering ion [25] or surface temperature effects are not included. Instead, all calculated sputtering yields were scaled by single free parameter factor, $\mathbf{F_Y}$, to match the experimental gross erosion rate.

The sputtered material redeposition flux was calculated by integrating the product of the outgoing flux from each location by a single redeposition probability distribution function (R_{PDF}). The model uses an asymmetric Lorentzian, defined by a width (***w***), skew term (λ), and normalized to a total redeposition fraction (F_R). This function allows a separation of the more complicated atomic and plasma physics processes, such as the sputtered atom energy and angular distribution, the ionization mean free path, collision and entrainment by background plasma, and drifts and acceleration through the sheath, from the material evolution given simple flux balancing. By fitting a general function to the observed data we gain insight into discrepancies between experimental observations and advanced modeling codes. The advanced Monte-Carlo erosion-deposition modeling code ERO [26] was used to calculate a deposition distribution for case Al4, using a uniform background plasma using measured parameters and a cosine sputtering angle distribution. Although a Bi-Lorentzian fits the predicted function well, the shape of the function required for a best fit to the data shows much higher asymmetry (Figure7). This discrepancy between ERO modeled deposition distribution function indicate that either the downstream plasma transport of Al is under-estimated in ERO, or that there is some asymmetry to the sputtered angle distribution in the experiment.

$$\varphi_{T,out}(x) = F_Y X_T(x) \sum_i S_{i\to T}\varphi_i \quad (1)$$

$$\varphi_{C,in} = F_C \varphi_D \quad (2)$$

$$\varphi_{Al,in}(x) = \int \varphi_{Al,out}(x+u) R_{redep}(x+u)du \quad (3)$$

$$R_{redep}(u) = F_{redep} \frac{2w(1\mp\gamma)/\pi(1\pm\gamma)}{4u^2+\left(w(1\mp\gamma)\right)^2} \quad (4)$$

$$dN_{surf}/dt = \left(1 - F_{trap}\right)\varphi_{T,in} - \varphi_{T,out} \quad (5)$$

$$dN_{trap}/dt = F_{trap}\varphi_{T,in} \quad (6)$$

Other factors not taken into account are the finite two dimensional size of the samples (currently only 1-D profiles are modeled), and a higher sputtering yield for redeposited material compared to the original coating. Future improvements are planned to extend the model to allow two-dimensions, improve the material mixing depth profile, and allow for spatially or temporally varying redeposition function determined from more rigorous ERO modeling with reconstructed divertor plasma parameters and various sputtering angle distributions.

4. Conclusion

We have measured both erosion and deposition of Al in divertor plasma contact using both in-situ and post-mortem techniques. We observed average gross erosion rates that were between 50 and 75% of the expected rate based on physical D (or He) and C impurity ion sputtering. Non-spectroscopic measurements of net and gross erosion from large and small areas suggest an effective net:gross erosion ratio of ~0.8 in these cases, but modeling of the erosion-deposition process was needed to include the effect of surface roughness on the total amount of eroded material found redeposited on the probe surface. The simple model presented here reproduces several of the experimental observations: the toroidal asymmetry in the net erosion rate; increased erosion rate from smaller areas; an accumulation of re-deposited material off the original coating primarily in the downstream toroidal direction; and higher accumulation rate of redeposited material on rough surfaces. The model reduces the measured erosion/deposition profile resulting from different sample geometries to a point-source like redeposition probability distribution function that represents the sputtering, ionization, and transport effects to help benchmark the physics processes included in more advanced modeling codes.

The results of the model interpretation suggest that about 30-45% of the eroded Al returns to the surface within 1cm of the original location, with higher fraction at higher n_e and T_e. However, due to re-

erosion, almost none of this redeposited Al is remains on the surrounding surface of a smooth substrate sample, while 50% of the redeposited material was accumulated on the rough substrate samples. The shape of the redeposition function needed to fit the data was more asymmetric than predicted by the ERO modeling code, suggesting either a more asymmetric sputtering angle distribution or stronger downstream plasma transport effect.

5. Acknowledgements

I would like to acknowledge Bill Wamlper for his development of the initial SAP erosion-deposition model, Dean Buchenauer and Bernnice Mills for sample preparation and surface analysis, Graham Wright for the detailed RBS measurements, and the DIII-D operations team for their support. Sandia National Laboratories is a multi-program laboratory managed and operated by Sandia Corporation, a wholly owned subsidiary of Lockheed Martin Corporation, for the U.S. Department of Energy's National Nuclear Security Administration under contract DE-AC04-94AL85000.

6. References

[1] S. Carpentier et al., J. Nucl. Mater. 415 (2011) S165–S169.

[2] R.P. Doerner et al., J. Nucl. Mater. 342 (2005) 63–67.

[3] J.H. Yu et al., Phys. Scr. T159 (2014) 014036.

[4] R. Ding et al., Nucl. Fusion 55 (2015) 023013.

[5] W.R. Wampler et al., Phys. Scr. T159 (2014) 014069.

[6] D. Borodin et al., Phys. Scr. T145 (2011) 014008.

[7] D. Naujoks et al., J. Nucl. Mater. 220-222 (1995) 227–230.

[8] L. Marot et al., Fusion Eng. Des. 88 (2013) 1718–1721.

[9] C.P.. Wong et al., J. Nucl. Mater. 258-263 (1998) 433–439.

[10] C.P.C. Wong et al., J. Nucl. Mater. 196-198 (1992) 871–875.

[11] P.C. Stangeby et al., J. Nucl. Mater. 316 (2008) 883–887.

[12] C. Chrobak et al., J. Nucl. Mater. 463 (2015) 810–813.

[13] D.L. Rudakov et al., Phys. Scr. T159 (2014) 014030.

[14] P.C. Stangeby, The Plasma Boundary of Magnetic Fusion Devices, IOP Publishing, 2000.

[15] J.N. Brooks et al., J. Nucl. Mater. 438 (2013) S673–S676.

[16] C. Chrobak et al., J. Nucl. Mater. 463 (2015) 810–813.

[17] M. Mayer et al., J. Nucl. Mater. 363-365 (2007) 101–106.

[18] S. Dai et al., Nucl. Fusion 54 (2014) 123015.

[19] K. Schmid et al., Nucl. Fusion 50 (2010) 105004.

[20] A. Kirschner et al., J. Nucl. Mater. 328 (2004) 62–66.

[21] R.P. Doerner et al., J. Nucl. Mater. 463 (2015) 777–780.

[22] W.R. Wampler et al., J. Nucl. Mater. 438 (2013) S822–S826.

[23] W.R. Wampler, in:, Plasma Facing Mater. Components Fusion Appl., 2015.

[24] A. Mutzke et al., SDTrimSP Version 5.00 IPP Report 12/8, Garching, 2011.

[25] R.P. Doerner et al., J. Nucl. Mater. 438, Suppl (2013) S272–S275.

[26] A. Kirschner et al., Nucl. Fusion 40 (2000) 989–1001.

Figures

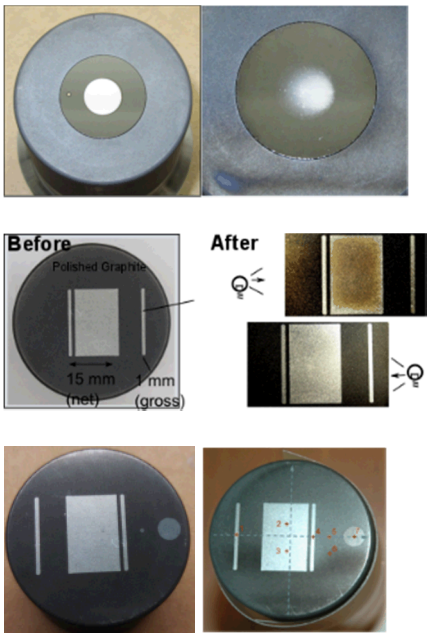

Figure 1. Pre and post-exposure images of Al1, Al4, and Al5 samples. Al1 sample was almost completely eroded during the exposure, and the 1mm spot was not found, but a higher erosion rate on the upstream edge of the coating is evident. Al4 and Al5 samples developed a non-isotropic reflectivity. Dark field imaging of the exposed Al4 sample using shallow angle illumination from the upstream (d) and downstream (e) directions reveals dark (net deposition) areas on the field-shadowed surfaces, and bright (net erosion) surfaces on the field-facing side. Sample Al5 included two additional areas coated with W, for the purpose of providing a measurement of erosion by C impurity in He plasmas.

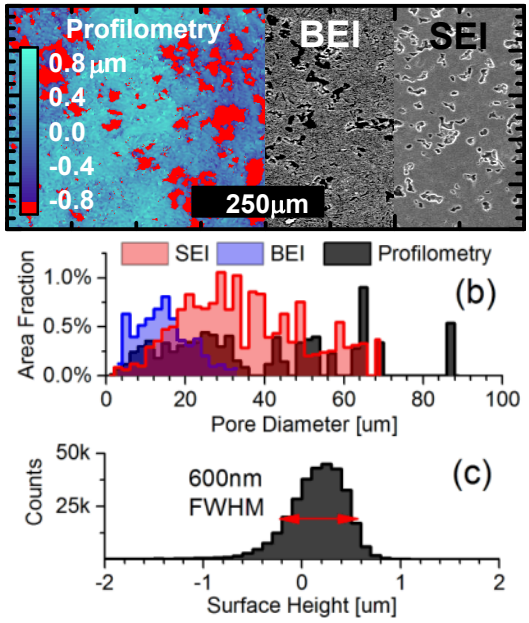

Figure 2: Profilometry image showing pores as red regions in the image compared with back-scattered electron imaging (BEI) and secondary electron imaging (SEI) of the porous Al-coated graphite surface. Distributions of pore sizes analyzed from these images (b) and the surface roughness from profilometry (c) shown.

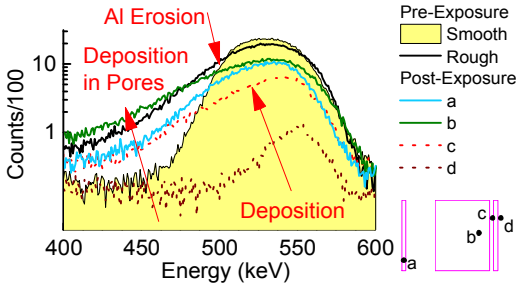

Figure 3. RBS spectra detailing Al peak measured on Al4 (rough) sample before and after exposure, compared to a smooth coating. The Al peak measured in areas of the coating with higher redeposition (b) has a wider low-energy tail peak shape than areas low redeposition (a).

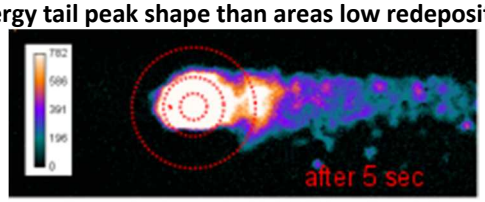

Figure 4: Images of AlI emission shows erosion from the original coating, re-erosion roughly symmetrical within 8mm, but long range redeposition and re-erosion exclusively in the downstream toroidal direction.

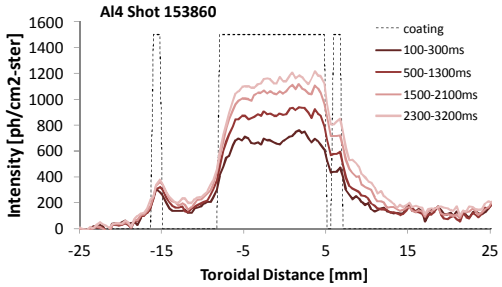

Figure 5: Observed profile of AlI emission for the first 3200ms of the Al4 exposure (shot 153860), proportional to sputtered neutral Al flux from the sample. We see relatively constant emission from the upstream 1mm coating, while emission from the downstream 10mm coating increases during the shot. The brightness downstream of the original coating also increases, indicating increasing re-erosion of redeposited material there.

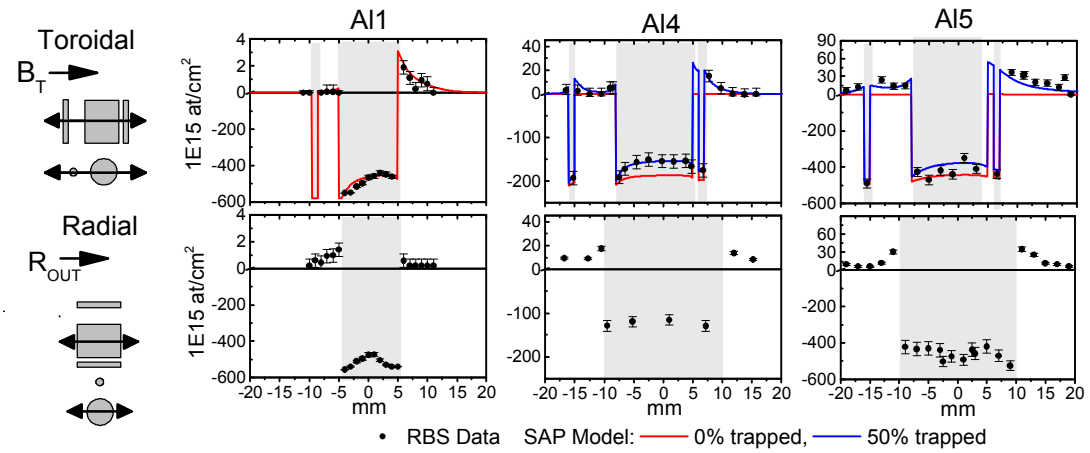

Figure 6: Toroidal and radial profiles of observed erosion for cases Al1 (Al and C), Al4 (Al) and Al5 (Al and W), with best fits using SAP model. Background impurities in the graphite limited the sensitivity to Al of ~5x10^{14} atoms/cm^2.

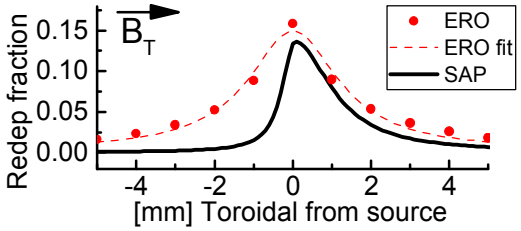

Figure 7. Redeposition distribution function (SAP) used to fit the observed toroidal erosion profile for case Al4 and (ERO) modeled by ERO for Al4 case plasma parameters using ADAS ionization rate coefficients and fit to a bi-lorentzian (ERO fit).

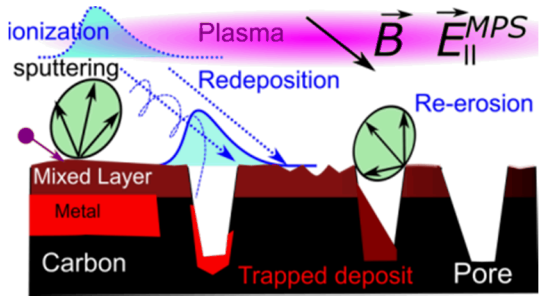

Figure 8. Diagram of erosion/deposition process calculated in the model. The model numerically integrates rate equations for metal & C loss or gain vs time. The surface concentration in the mixed layer is updated using the redeposition flux of Al and background C ion flux, and the process is repeated.